In-Situ Studies of Structure Development during the Reactive Processing of Model Flexible Polyurethane Foam Systems Using FT-IR Spectroscopy, Synchrotron SAXS, and Rheology

Michael J. Elwell[†] and Anthony J. Ryan*

Manchester Materials Science Centre, UMIST, Grosvenor Street, Manchester M1 7HS, United Kingdom

Henri J. M. Grünbauer and Henry C. Van Lieshout

Urethanes Research and Development, Dow Benelux N.V., Herbert H. Dow Weg, Postbus 48, 4530 AA Terneuzen, The Netherlands

Received July 31, 1995; Revised Manuscript Received December 11, 1995[⊗]

ABSTRACT: FT-IR spectroscopy, synchrotron SAXS, and dynamic rheometry have been employed to monitor, *in-situ*, structure development during the reactive processing of model flexible polyurethane foam systems. The following combinations of components were investigated: (I) diisocyanate, polyether polyol, and water and (II) diisocyanate, polyether monol, and water. The formation of urethane, soluble urea, and hydrogen-bonded urea species during the fast bulk copolymerization has been studied using the adiabatic reactor method and forced-adiabatic, time-resolved FT-IR spectroscopy. The decay of isocyanate is correlated with the polymerization kinetics, and the evolution of hydrogen-bonded urea is analyzed emphasizing the onset of microphase separation of urea hard segment sequences. FT-IR spectroscopy indicated that the microphase separation transition (MST) occurred at a critical conversion of isocyanate functional groups and followed the kinetics associated with nucleation and growth. The dynamics of microphase separation during the fast bulk copolymerization have also been investigated employing forced-adiabatic, time-resolved synchrotron SAXS experiments. Microphase separation was observed to occur at a critical conversion of isocyanate functional groups and is shown to follow the kinetics associated with spinodal decomposition. Forced-adiabatic rheological measurements have been conducted during the fast bulk copolymerization. Four main regions of rheological development during the formation of polyurethane foam were identified. These were: (I) bubble nucleation, (II) liquid foam and microphase separation, (III) physical gelation, and (IV) foamed elastomer. The use of model systems demonstrated that the presence of covalent cross-links delay the onset of microphase separation of the urea hard segment sequence lengths. Although foam stability is not dependent upon the formation of urethane covalent cross-links in the early part of the foaming reaction, molecular connectivity between the microphases via urethane covalent cross-links is an essential requirement with regard to long-term dimensional stability and the mechanical/physical properties of the foam.

Introduction

The reactive processing of water-blown flexible polyurethane foam from liquid monomers and oligomers involves a complex combination of both chemical and physical events. In less than 5 min, a liquid mixture of relatively low molecular weight components is transformed into the supramolecular architecture of solid a foam. Information regarding both the reaction kinetics and development of morphology during processing is essential, such that an objective description of the events taking place and, ultimately, selective control of the process can be achieved. Flexible polyurethane foam is formed by the simultaneous reaction between a diisocyanate with polyether polyol and water. Combination of these two exothermic reactions leads to the formation of a segmented block copoly(urethane−urea) of the $-(H_mS)_n-$ type. This is blown into a foam by the cogeneration of carbon dioxide gas evolved from the water−isocyanate reaction. As the polymerization proceeds, the core of the rising foam bun becomes self-insulated by the surrounding polymer and this results in the process occurring under quasi-adiabatic conditions. Reaction kinetic studies during foam formation with both tolylene diisocyanate (TDI) and methylene bis(phenyl isocyanate) (MDI) have been conducted previously and the results are in the literature.[1−5]

Analyses[6−8] of the final morphology present in flexible polyurethane foams employing small-angle X-ray scattering (SAXS), dynamic mechanical spectroscopy (DMS), and differential scanning calorimetry (DSC) have shown them to exhibit a microphase-separated morphology similar to that of segmented urethane elastomers. The development of morphology during foaming is complex.[3] As the chemical reactions proceed, the chain lengths (N, degree of polymerization) of all the products increase and the interaction parameters (χ) can also change. Such changes can give rise to the system crossing thermodynamic boundaries which results in a transition from an initial homogeneous (disordered) state into a microphase-separated (ordered) state.[9,10] The resultant morphology is determined by the kinetic competition between polymerization and microphase separation.[7,9,10] *In-situ* investigations regarding the reaction kinetics and development of polymer structure in both flexible and rigid polyurethane foam are sparse.[3,5,11,12]

Model reactions have been employed previously to investigate the reaction kinetics in urethane systems.[13−20] As far as we are aware, there are only five studies[1,21−24] in the literature where model reaction systems have been employed to study the development of polymer morphology in urethane foams. Rossmy and coworkers[21−23] showed that urethane formation in the

* Author to whom correspondence should be addressed.
[†] Current address: Urethanes Research and Development, Dow Benelux N.V., Herbert H. Dow Weg, Postbus 48, 4530 AA Terneuzen, The Netherlands.
[⊗] Abstract published in *Advance ACS Abstracts,* March 1, 1996.

0024-9297/96/2229-2960$12.00/0 © 1996 American Chemical Society

Table 1. Details of the Formulations Employed for the Forced-Adiabatic, Time-Resolved FT-IR Spectroscopy, Synchrotron SAXS, and Dynamic Rheometry Measurements during the Foaming Reaction

foaming system	% by weight hard segment	mass of polyol or monol/g	mass of isocyanate/g	mass of catalyst/g	mass of water/g	mass of silicone surfactant/g
PU-220	24.5	100	38.7	0.70	2.20	0.80
PU-220-MONOL	24.4	100	38.7	0.70	2.20	0.80
RIMSAXS-210	23.5	100	37.1	0.70	2.10	4.00
RIMSAXS-210-MONOL	23.5	100	37.1	0.70	2.10	4.00

early part of the foaming reaction was not important with regard to foam stability by the synthesis of foams from both reactive and nonreactive polyethers. Such foams showed sufficient internal modulus to withstand foam collapse and support their own mass. Hocker[24] reported that the carbonyl group that is present in soluble urea (1715 cm^{-1}) interacts sooner with urethane carbonyls (1730 cm^{-1}) than that of soluble D-urea (1697 cm^{-1}). The use of deuterium oxide instead of water results in a shifting of the soluble D-urea and associated D-urea absorbance peaks to lower wavenumbers. This facilitates exposure of the urethane absorbance peak, which was partly obscured by the soluble urea peak in the systems where water was used. The use of deuterium oxide enables the presence of hydrogen-bonded urethane species to be probed as a result of the large reduction in the extent of peak overlap. More recently, Artavia and Macosko[1] have used deuterium oxide for investigating microphase separation of D-urea hard segment sequence lengths under isothermal and forced-adiabatic conditions via FT-IR spectroscopy during foam formation.

In order to understand more fully the reaction chemistry and subsequent structure development processes during foam formation, model foaming reactions employing a monofunctional polyether have been investigated. In foam formulations which commonly employ a nominally trifunctional polyether polyol, this component has been substituted for a monofunctional polyether (or monol) of the same chemical composition as the polyether polyol (i.e., effectively one arm of the polyether polyol). Monol foams have no urethane covalent cross-links, which enables their effect on the structure development processes to be investigated.

To study the polymerization of flexible polyurethane foam, *in-situ*, via FT-IR spectroscopy, synchrotron SAXS or rheometry is difficult. The material undergoes an exotherm of 75−150 °C, the viscosity of the reaction medium increases from ≈10 to 10^4 Pa s, and the density decreases from 1000 to 30 kg m^{-3} or less in under 4 min. Although the conversion of the component monomers can be evaluated from the adiabatic temperature rise profile, this reveals nothing about the reaction chemistry sequence, morphological changes, or macroscopic properties as a function of the extent of reaction. However, if information about the system is required in terms of the sequence of chemical reactions taking place, changes in the sample morphology, or the development of macroscopic properties as a function of the extent of reaction, a major problem arises. The problem is the nature of the sampling environment, as a small mass of material in an unheated cell will suffer heat loss (the cell acts as a heat sink) and, as a consequence, will decrease the foam reaction exotherm, delay the reaction chemistry, and disrupt the resulting morphological development. This problem has been overcome by the design and use of temperature-controlled reaction cells and rheometer plates. A discussion regarding the design and operating conditions of these devices is documented elsewhere.[1,2,4,25] In this paper, results are presented from investigations in which FT-IR spectroscopy, synchrotron small-angle X-ray scattering (SAXS), and dynamic rheometry have been used under forced-adiabatic conditions to observe how the multiphase polymer structure evolves during foam formation in model, MDI-based flexible polyurethane foam systems.

Experimental Section

Materials. Two formulations have been employed: (1) polyol−water and (2) monofunctional polyether−water reacting with diisocyanate. Both are based upon 100.0 g of polyol by convention. An isocyanate index of 105 was maintained throughout the work. Formulation details are reported in Table 1. Further details regarding the reactants are described elsewhere.[4] Both foaming systems were tested in triplicate for each experiment. All chemicals were used as supplied.

FT-IR Spectroscopy. Van Lieshout and Grünbauer[4,11] have developed a forced adiabatic FT-IR cell where sampling takes place outside the spectrophotometer. Details of the experimental arrangement and procedures adopted are documented elsewhere[4].

Synchrotron SAXS. The SAXS measurements were made on beam line 8.2 at the Synchrotron Radiation Source (SRS), Daresbury Laboratory, Warrington, UK. Further details regarding the configuration of the beam line, the experimental procedures adopted, and data analyses have been described elsewhere.[12] Reaction injection molding (RIM)[26] was employed to remotely meter, mix, and inject the reaction mixture into the SAXS reaction cell.[27] A temperature-controlled reaction cell has been designed[12] which can be positioned in the optical bench assembly of a synchrotron beam line and fed with a pseudovirgin reaction mixture from a micro-RIM machine.[12,27−29] The specifications of the SAXS sampling cell, the experimental arrangement, and the procedures adopted are described elsewhere.[5,12]

Dynamic Rheometry. The application of electrical heating devices built into/around the disposable fixtures/plates for rheometers has been reported previously.[30−32] A forced-adiabatic rheometer plate that can be attached to a modified lower fixture for the Rheometrics RMS 800 series rheometer has been constructed recently in our laboratory; the specifications of the temperature-controlled rheometer plate, the experimental arrangement, and procedures adopted are described elsewhere.[25]

Results

FT-IR Spectroscopy. Figure 1 shows the basic reaction chemistry taking place during foam formation.[4] The isocyanate absorption band occurs at approximately 2300−2270 cm^{-1} in the mid-infrared spectrum, and the decay in the intensity of this absorbance can be used to monitor the conversion of isocyanate functional groups during the reaction. Figure 2a is a three-dimensional plot of the isocyanate absorbance versus frequency versus time for the foaming system PU-220. It shows clearly the decay in the intensity of the isocyanate absorbance with time. Each spectrum was recorded at 6 s intervals. Figure 2b shows a similar three-dimensional plot for the corresponding carbonyl region of the foaming system PU-220, illustrating the evolution of urethane, soluble urea, and hydrogen-bonded urea.[4] It is apparent that urethane (≈1730 cm^{-1}) and soluble urea (≈1715 cm^{-1}) evolve early in the reaction. These

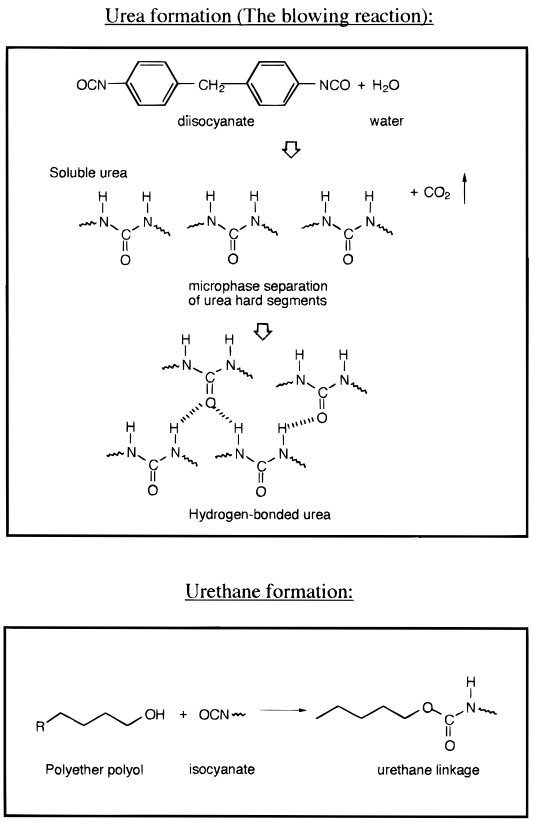

Figure 1. Schematic representation of the reaction chemistry taking place during polyurethane foam formation.

two reactions take place simultaneously: not sequentially, as early research had suggested.[22,33,34] It is also apparent that there is an induction time prior to the evolution of hydrogen-bonded urea (≈1654 cm^{-1}).

Assuming that there are no side reactions,[1,4] the only source of heat during the foaming reaction is that arising from the consumption of isocyanate functional groups. It is thus possible to correlate the isocyanate conversion calculated from the decay in the isocyanate absorption with time, and that calculated from normalisation of the reaction exotherm.[1,4] Figure 3 compares isocyanate conversion calculated from the forced-adiabatic spectroscopy data (open symbols) with that calculated from the normalization of the foam reaction exotherm (solid line) for the foaming systems PU-220 and PU-220-MONOL. The correlation between the isocyanate conversion calculated from adiabatic temperature rise and infrared spectroscopy data is within ±3% after approximately 40 s of the reaction. It should be considered that the first 15 s depicted on the aforementioned curves is associated with mixing of the components and loading of the reaction mixture into the infrared cell arrangement.

Figure 4 shows representative plots of normalized soluble urea (1715 cm^{-1}, open symbols) and hydrogen-bonded urea (1654 cm^{-1}, closed symbols) versus reaction time for the foaming systems PU-220 and PU-220-MONOL. The soluble urea and hydrogen-bonded urea absorbance bands were normalized against isocyanate conversion. The normalization is carried out because the probe (carbonyl) concentration is directly proportional to conversion. The normalization removes the change in concentration effect. The onset of microphase separation (MST) is indicated with an arrow and is taken as the point at which there is an acceleration in the hydrogen-bonded urea and a depletion in the free

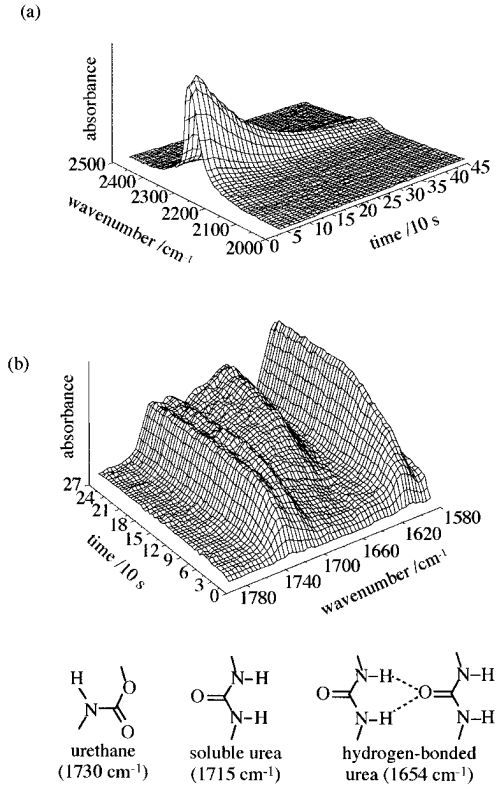

Figure 2. (a) Three-dimensional surface plot of the isocyanate absorbance versus frequency, versus time for PU-220. (b) Three-dimensional surface plot of absorbance versus frequency versus time for the region 1780−1580 cm^{-1} in the mid-infrared spectrum for PU- 220. The absorbances associated with urethane, soluble urea and hydrogen-bonded urea are indicated. The absorbance at ≈1600 cm^{-1} is that associated with >C═C< in plane vibration of the benzene ring.

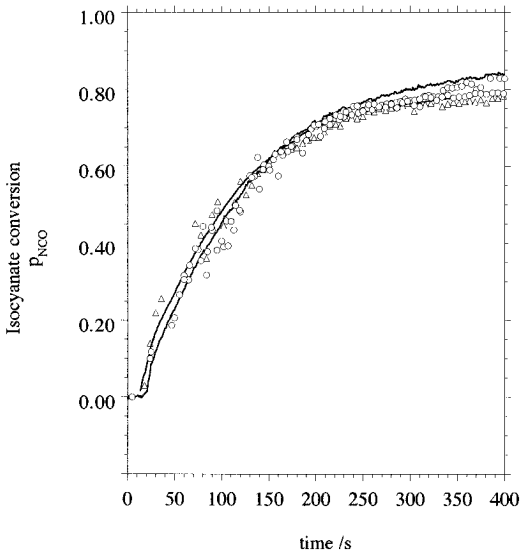

Figure 3. Isocyanate conversion as a function of time showing the correlation between infrared spectroscopy data (open symbols) and adiabatic temperature rise data (solid lines) for PU-220 (○) and PU-220-MONOL (△).

urea.[1,29] At the MST, the system becomes both chemically and spatially heterogeneous, and this separates functional groups.

It has been observed[4] for polyol systems that across a broad range of water concentrations the conversion of isocyanate functional groups at the MST remains approximately constant at $p_{NCO} = 0.55 \pm 0.05$. Thus, the critical isocyanate conversion at which the local

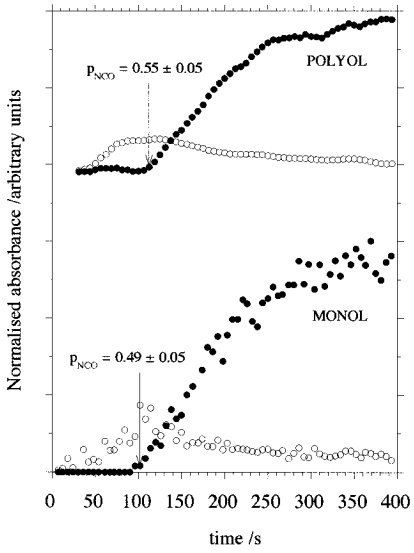

Figure 4. Normalized soluble urea (open symbols) and normalized hydrogen- bonded urea (closed symbols) as function of time for PU-220 and PU-220-MONOL. The location of the MST is marked with a vertical arrow.

number-average hard segment sequence length, N_H, reaches N_{Hcrit} is approximately 55 ± 5% conversion of isocyanate functional groups. This corresponds to an average hard segment sequence length of 1.1−1.5 units.[5] From Figure 4 it may be deduced that a similar type of structuring process occurs in PU-220-MONOL as was observed in PU-220. Microphase separation *seems* to occur at a lower isocyanate conversion in PU-220-MONOL than in PU-220. However, the difference lies on the boundaries of the limits for experimental error. FT-IR studies show that when the water is replaced by deuterium oxide, microphase separation *does* occur at a lower isocyanate conversion in the monol system compared with the polyol system.[35] The higher overall conversion of isocyanate in the polyol system compared to the monol system is a result of macrophase separation of urea hard segment sequences in the monol system, which separates functional groups. This has been discuused in detail elsewhere.[35]

Synchrotron SAXS. Representative time-resolved SAXS data that have been collected during foam formation (at 2 s intervals) are presented in Figures 5a and 5b for RIMSAXS-210[12,36] and RIMSAXS-210-MONOL, respectively. For the purpose of clarity, only every fourth time frame is shown. They are three dimensional surface plots of intensity, $I(q,t)$, versus scattering vector, q, versus time, t. The patterns for both systems illustrate that in the early stage of the reaction there is a homogeneous liquid present. At the microphase separation transition (MST), there is the first appearance of a scattering maxima and the intensity of this peak continuously increases. Eventually, the growth slows down and the peak intensity becomes approximately constant. This is after the expanding foam has reached the Berghmans point,[37] where microphase separation is intercepted and arrested by vitrification of the phase that is richer in hard segment. The maximum in $I(q)$ suggests the presence of structure with periodic electron density within the sample. For the foaming system RIMSAXS-210, the maximum in $I(q)$ occurs at $q \approx 0.06$ Å^{-1}, giving an interdomain spacing of 105 Å. For the foaming system RIMSAXS-210-MONOL, the interdomain spacing was calculated to be 103 Å. The d spacing did not change during the structuring process for either system.

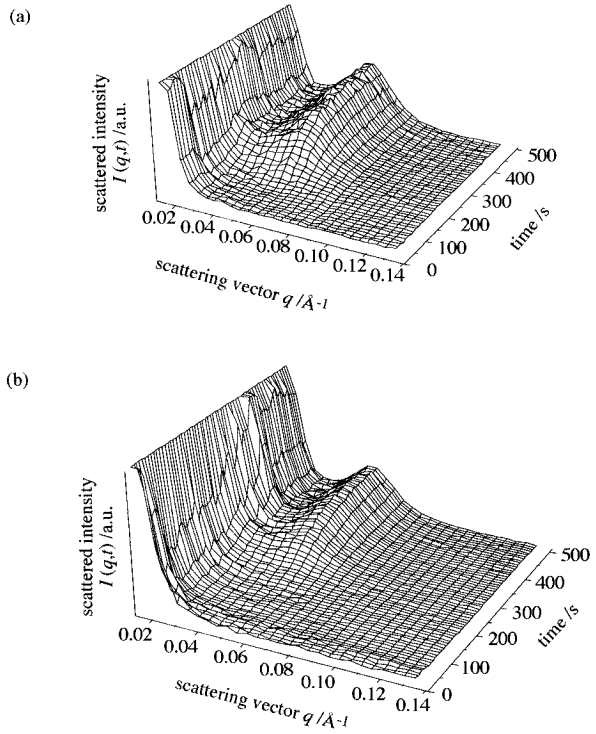

Figure 5. Three-dimensional surface plot of scattered intensity, $I(q,t)$, versus scattering vector, q, versus reaction time, t, of a representative data set for (a) RIMSAXS-210 and (b) RIMSAXS-210-MONOL.

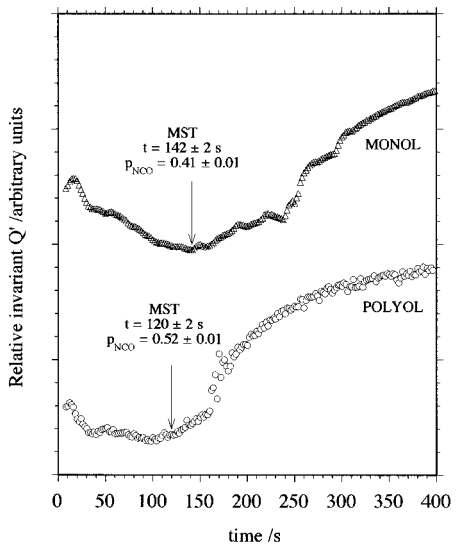

Figure 6. Plot of representative data sets of the relative invariant, Q', as a function of time for RIMSAXS-210 and RIMSAXS-210-MONOL. The location of the microphase separation transition is also indicated.

Figure 6 shows representative plots of the relative invariant, Q' (a measure of the degree of microphase separation),[12] versus reaction time. For the foaming system RIMSAXS-210, the onset of microphase separation is taken as 120 ± 2 s. This corresponds to an isocyanate conversion $p_{NCO} = 0.52 \pm 0.01$. For the foaming system RIMSAXS-210-MONOL, the onset of microphase separation is taken as 142 ± 2 s. This corresponds to an isocyanate conversion $p_{NCO} = 0.41 \pm 0.01$. For multiple runs on both the polyol- and the monol-based systems, the onset of microphase separation occurred at $p_{NCO} = 0.54 \pm 0.02$ for the polyol and $p_{NCO} = 0.42 \pm 0.02$ for the monol. The invariant data for the monol are intrinsically more noisy than for the

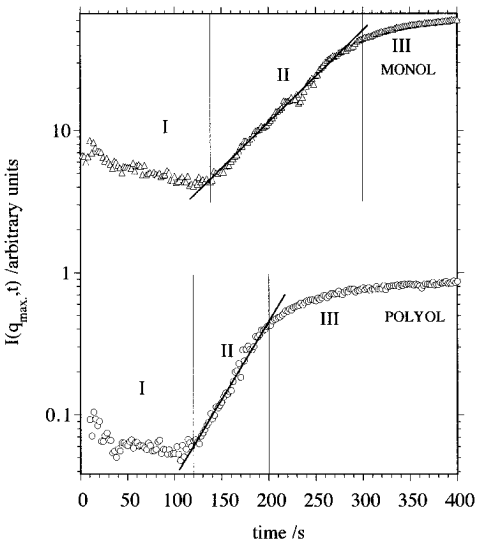

Figure 7. Plot of the density corrected, peak intensity, $I(q_{max.},t)$, versus time, t, for RIMSAXS-210 and RIMSAXS-210-MONOL. The symbols are experimental data points and the solid line is a logarithmic fit (after Cahn and Hilliard[42]).

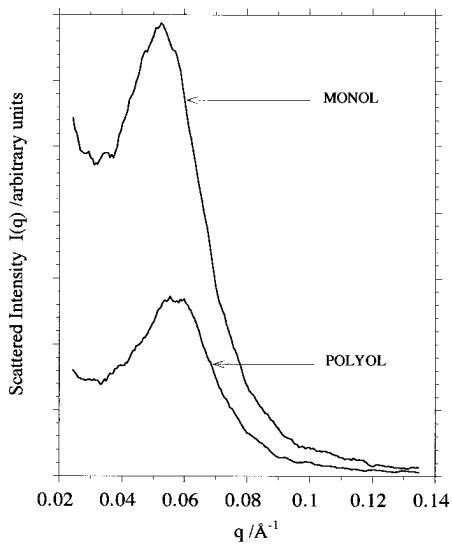

Figure 8. Plot of the scattered intensity, $I(q,t)$, versus scattering vector, q, after 500 s of reaction; for representative data sets of RIMSAXS-210 and RIMSAXS-210-MONOL.

polyol because monol foams are unstable during the bubble growth process and continually collapse; thus less material is scattering, giving a poorer signal to noise ratio. The driving force for microphase separation is the thermodynamic incompatibility between the hard and soft segment blocks.[9,10,27,38−40] As polymerization proceeds, the degree of polymerization of the hard segment, N_H, increases. For RIMSAXS-210 at $p_{NCO} = 0.54 \pm 0.02$ and for RIMSAXS-210-MONOL at $p_{NCO} = 0.42 \pm 0.02$, the number-average hard segment sequence length reaches a critical value and the product χN_H (where χ is the Flory−Huggins interaction parameter) is such that the system is no longer thermodynamically stable [i.e., $\Delta G \geq 0$ and $(\partial^2 \Delta G/\partial \phi_H^2) \leq 0$]. The polymerization has acted as a large thermodynamic quench. The depth of this quench determines the mechanism by which microphase separation occurs.

The material that starts to form structure is a combination of homopolymer, block copolymers, and monomers and is discussed in terms of a mixture. The final structured material is predominantly a block copolymer, and thus the data are also analyzed in terms of the TDGL theory for microphase separation.[41] Depending upon the route a mixture follows through phase space, two very distinct mechanisms of phase separation are observed: nucleation and growth, and spinodal decomposition.[9,39,40,42] Figure 7 shows representative plots of the peak intensity, $I(q_{max.},t)$, as a function of time for the foaming systems RIMSAXS-210 and RIMSAXS-210-MONOL. From the two curves, there appear to be three distinct regions of phase behavior. These can be interpreted in the following way.

Region I: This is a homogeneous liquid mixture comprised of unreacted monomer, homopolymer, urea hard segment sequences, and isocyanate-tipped, polyether oligomers.

Region II: This is the microphase separation transition (MST). At the MST there is observed a rapid increase in the scattered intensity. There is a good fit of the data to an exponential increase in intensity with time. This is a characteristic of phase separation via spinodal decomposition.[42] The slope of the line provides a measure of the amplification rate, $R(q)$, of the composition fluctuations.[38,41]

Region III: The expanding foam has reached the Berghmans point[37] (onset of vitrification) and beyond this, the scattered intensity remains approximately constant.

Vitrification of the hard segments freezes in the morphology at that time and results in the evolution of a foam with an internal polymer morphology that comprises an interconnecting physical network of hydrogen-bonded urea hard segment sequences within *a cross-linked polyether-urethane* in the case of RIMSAXS-210. For RIMSAXS-210-MONOL, the internal polymer morphology for the greater part is an interconnecting physical network of hydrogen-bonded urea hard segment sequences within *a polyether−urethane*, but dispersed within the interconnecting physical network of hydrogen-bonded urea hard segment sequences and polyether−urethane are isolated larger aggregates of hydrogen-bonded urea hard segment sequences. Figure 8 shows representative plots of the scattered intensity, $I(q,t)$, versus scattering vector, q, after 500 s of reaction for the polyol and monol systems. The rapid increase in magnitude of $I(q,t)$ at low values of q in the case of the monol suggests the presence of larger dispersed particles. Furthermore, the level of phase separation in the monol system is higher than that in the polyol system.

To aid in the interpretation of the mechanism of phase separation, the scattering patterns taken during the reaction have been analyzed to obtain the composition amplification rate at discrete wave vectors, $R(q)$. For microphase separation via spinodal decomposition, a plot of $R(q)/q^2$ (a measure of the thermodynamic driving force for phase separation)[5,12,36,38,41] versus q^2 should exhibit a maximum at a finite value of q.[38,41] Figure 9 shows representative plots of $R(q)/q^2$ versus q^2 for the systems RIMSAXS-210 (closed symbols) and RIMSAXS-210-MONOL (open symbols). From the peak in the curve[12] of RIMSAXS-210, the effective diffusion coefficient, D_{eff}, of the polyether soft segment (polyol system) was calculated to be -4.9 ± 0.3 Å^2 s^{-1}. The negative diffusion coefficients indicate diffusion against the composition gradient (i.e., from a region of low concentration to a region of high concentration) as found in spinodal decomposition of a mixture.[39,40,42] For the foaming system RIMSAXS-210-MONOL, no maximum

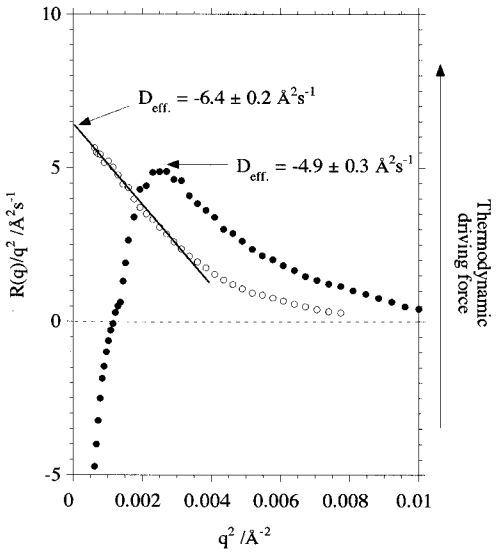

Figure 9. Plot of $R(q)/q^2$ vs q^2 for representative data sets of RIMSAXS-210 (●) and RIMSAXS-210-MONOL (○).

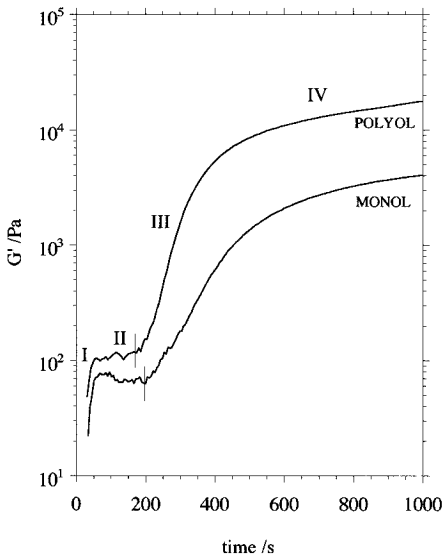

Figure 10. Plot of representative data sets of the elastic shear modulus, G', for RIMSAXS-210 and RIMSAXS-210-MONOL. Four regions of rheological development can be identified.

in $R(q)/q^2$ versus q^2 is observed. The linear behavior at low values of q can be extrapolated to $q^2 = 0$, allowing the effective diffusion coefficient, D_{eff}, of the polyether soft segment (monol system) to be calculated. A value of -6.4 ± 0.2 Å^2 s^{-1} was obtained for D_{eff}. This type of behavior suggests that the monol system is similar to that of a macrophase-separated polymer blend/mixture rather than a microphase-separated block copolymer. Similar behavior was observed by Bates and Wiltzius[43] for a mixture of protonated and deuterated 1,4-poly(butadiene).

The one major difference between the monofunctional-based system and the nominally trifunctional-based system is that molecular connectivity exists between two microphases of the same type in the polyol-based system. The important result that emerges from the analysis is that for the foaming system RIMSAXS-210, the microphase separation kinetics can be qualitatively described by the time-dependent Ginzburg−Landau model described by Hashimoto.[41] This provides very strong evidence in favor of microphase separation proceeding via a spinodal decomposition type process during the foaming reaction. For the foaming system RIMSAXS-210-MONOL, the scattering data strongly suggest that the mechanism is macrophase separation via a spinodal decomposition and that the final structured material is a macrophase-separated mixture of diblock copolymer, homopolymer, and monomers. This would suggest that the internal morphology of RIMSAXS-210-MONOL is, for the greater part, similar to that of RIMSAXS-210, but dispersed within the interconnecting physical network of hydrogen-bonded urea hard segment sequences and polyether−urethane are isolated larger aggregates of hydrogen-bonded urea hard segment sequences.

Dynamic Rheometry. Mora and coworkers[30,31] and more recently Neff and Macosko[32] have identified four main regions of rheological development during the formation of polyurethane foam. Figure 10 shows representative plots of elastic shear modulus, G', versus reaction time for the foaming systems RIMSAXS-210 and RIMSAXS-210-MONOL. Also indicated on the figures are the four regions of rheological development. However, the interpretation here is slightly different from that of Mora and Artavia.[3,30,31]

Region I: Bubble Nucleation. In this stage, the dissolved bubbles of air that were "whipped" into the system during mechanical agitation act as nucleation sites for the carbon dioxide gas that is generated from the water−isocyanate reaction. These bubbles then develop into a space-filling network as observed previously by Kanner and Decker.[44] The initial viscosity is determined by the monomer viscosity.

Region II: Liquid Foam and Microphase Separation. For the foaming system RIMSAXS-210; at the end of region I the reacting mixture has an elastic shear modulus of approximately 100 Pa ($G' > G''$) and shows solid-like behavior which is a characteristic of liquid foams.[45,46] For the foaming system RIMSAXS-210-MONOL the reacting mixture has an elastic shear modulus of approximately 60−80 Pa ($G' > G''$). The data do not display the same degree of reproducibility as that of RIMSAXS-210 and are much noisier, most likely due to the reduced bubble stability. The reacting mixture in both cases is still a low-modulus gel that continues to expand as a result of the continued generation of carbon dioxide. The gel is formed from the interaction of closely packed bubbles. The liquid cell walls still have both low molecular weight and viscosity. For RIMSAXS-210, at approximately 120 s (isocyanate conversion is of the order of 54 ± 2%) microphase separation of urea hard segment sequences takes place as evidenced from SAXS measurements (see Figures 5−8) and infrared measurements (see Figure 4).

Beyond the MST, the foam modulus still remains approximately constant. For RIMSAXS-210-MONOL, at approximately 140 s (isocyanate conversion is of the order of 42 ± 2%) macrophase separation of urea hard segment sequences takes place as evidenced from SAXS measurements (see Figures 5−7) and infrared measurements (see Figure 4). It has been reported, however, that the change in modulus associated with the MST of polyolefins[47−49] and in one case of polyurethane[50] is of the order of a factor of 2. There are three contributions to there being no apparent change in the modulus at the MST for both the polyol and the monol. First, the material temperature is continuously changing (quasi-adiabatic). Second, the phase transition is not a particularly sharp one and is smeared even further by the polydisperse nature of the hard segment sequences.

Finally, the polymer is at a volume fraction of ≈0.1 at the MST and it is estimated that the increase in modulus of the polymer at the MST would give rise to a change in the foam modulus of ≈2%.

Region III: Physical Gelation. For RIMSAXS-210, at the end of region II the isocyanate conversion is of the order of approximately 70 ± 1%. At the start of region III there is a large increase in the elastic storage modulus, G', of approximately 2 decades. This increase in modulus results from microphase separation being intercepted and arrested by vitrification of the phase that is richer in urea hard segment. This is the Berghmans point.[37] Toward the end of region II, cell opening occurs. For RIMSAXS-210-MONOL, at the end of region II the isocyanate conversion is of the order of approximately 69 ± 1%. At the start of region III there is an increase in the elastic storage modulus, G', by a factor of 25.

Region IV: Foamed Elastomer. In polyurethane foam, after cell opening has occurred, the reactions still continue but do so in a medium of increasing viscosity and stiffness. Further increases in modulus and elasticity of the polymer due to vitrification of the hard segments and formation of covalent cross-links will severely restrict the escape of carbon dioxide from the foam. The cell membranes that have not previously ruptured will undergo reversible expansion, not rupture, and remain *closed cells*. In this region, the foamed polymer reaches maximum temperature and modulus. The modulus of the foam in this region is dominated by the polymer modulus. A similar behavior is displayed by RIMSAXS-210-MONOL; but in this system, covalent cross-links are not formed. Dynamic rheological measurements probe the macrocopic behaviour of the sample, not the molecular level (FT-IR, SAXS). In the case of the monol system, the lower and more erratic increase in modulus at the Berghmans point and the lower overall value of the elastic shear modulus result from macrophase separation within this system. The macrophase-separated aggregates of urea hard segment sequences are not connected to the physical network of hydrogen-bonded urea hard segment sequences, and, as such, they do not contribute to the polymer modulus. Thus, the final value of the modulus of the foamed polymer is lower than that observed in the polyol-based system.

In the polyol-based system, polymerization proceeds and from an early stage in the reaction there are isocyanate-tipped polyether oligomers and urea hard segment sequences present in the system (refer to Figure 2). The degree of polymerization of hard segment, N_H, increases steadily and at $p_{NCO} = 0.54 \pm 0.02$, N_H reaches N_{Hcrit} ($N_{Hcrit} \approx 1.5$ units)[5] and microphase separation takes place (refer to Figures 5−7). Polymerization has provided the thermodynamic quench passing from the homogeneous (disordered) one-phase region to the heterogeneous (ordered) two-phase region. For the case of the polyol, the isocyanate conversion at the MST ($p_{NCO} = 0.54 \pm 0.02$) is higher than that for the monol ($p_{NCO} = 0.42 \pm 0.02$). This behavior can be predicted from the theory of block copolymer thermodynamics proposed by Leibler[51] and Benoit and Hadzioannou.[52] For a diblock copolymer (the monol system) $\chi N_{crit} \approx 10$, but for a multiblock (the polyol system), $\chi N_{crit} \approx 15$. In the context of this paper, the more covalent bonds that exist between blocks, the higher the molecular weight obtained before ordering takes place. Put another way, as the polymer molecular weight increases, so does N_{Hcrit}.[27] The microphase-separated hard segments continue to grow and association of these urea hard segments occurs[4,12,36] (refer to Figure 4). At $p_{NCO} = 0.71 \pm 0.02$ (refer to Figure 10) microphase separation is intercepted and quickly arrested by vitrification of the phase that is richer in hard segment.[4,35,36] This phase has attained a composition with a T_g equal to the temperature of the reacting system. It is the composition where liquid−liquid phase separation is intercepted and arrested by glass transition and is termed the Berghmans point.[37] In general foam terminology, it is the physical gel point or end of rise time. Vitrification of the hard segments "freezes in" the morphology at that time and results in the evolution of a foam with an internal polymer morphology that comprises an interconnecting physical network of hydrogen-bonded urea hard segment sequences within the cross-linked polyether−urethane.[5,12,36]

In the monofunctional polyether system, the situation is somewhat different. Polymerization proceeds and in the early stages of the reaction there are isocyanate tipped polyether oligomers and urea hard segment sequences present in the system.[5,35,36] The degree of polymerization of hard segment, N_H, increases steadily and at $p_{NCO} = 0.42 \pm 0.02$, N_H reaches N_{Hcrit} ($N_{Hcrit} \approx 1.05$ units)[5] and macrophase separation takes place[5,35,36] (refer to Figures 5−7). The macrophase-separated urea hard segments continue to grow and association of these urea hard segments occurs[4,5,12,36] (refer to Figure 4). For the monol system, the rate of association of urea hard segments is approximately 33% faster than in the polyol system. This evidence is provided by values obtained for the effective diffusion coefficients from the *in-situ* synchrotron SAXS measurements. [D_{eff} of the polyether soft segment (polyol system) was calculated to be -4.9 ± 0.3 Å^2 s^{-1}. D_{eff} of the polyether soft segment (monol system) was calculated to be -6.4 ± 0.2 Å^2 s^{-1}.] Due to the very much faster rate of association of the urea hard segments, aggregates of urea hard segments are formed which cannot be stabilized by the MDI-tipped soft segment oligomers acting as a surfactant. As a result, these aggregates are macrophase separated, not connected to the polyether via a urethane linkage.

At $p_{NCO} = 0.69 \pm 0.01$, phase separation is intercepted and arrested by vitrification of the phase that is richer in hard segment. The internal polymer morphology of the polyether monol foam system is for the greater part, similar to that of the polyether polyol foam system.[12,35,36] Also dispersed within the interconnecting physical network of hydrogen-bonded urea hard segment sequences and polyether−urethane are isolated, larger aggregates of hydrogen-bonded urea hard-segment sequences (refer to Figure 8).

Summary and Conclusions

In this paper, we have described how the techniques of FT-IR spectroscopy, synchrotron SAXS, and dynamic rheometry can be used to investigate *in-situ* the development of polymer morphology during the reactive processing of flexible polyurethane foam. Each technique yields structural information of a different nature. The changes in the key structure parameters as isocyanate conversion increases can be summarized in a single diagram, and these are illustrated in Figures 11 and 12 for the polyol and monol systems, respectively.[5] It will be apparent that the SAXS relative invariant, Q', *appears* (within the limits of experimental error) to start to increase prior to the rapid growth in the

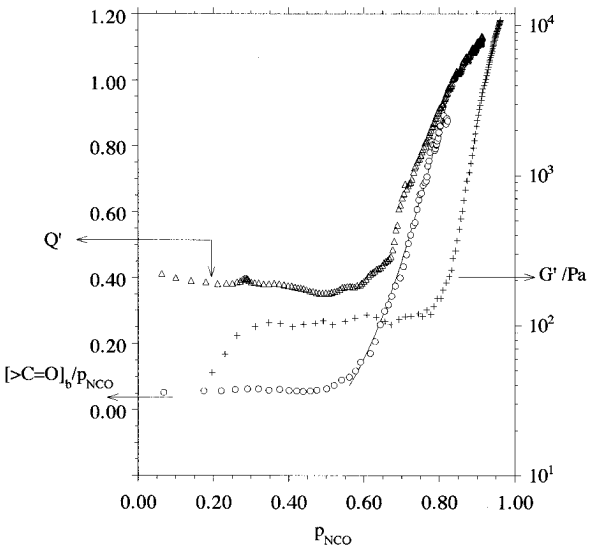

Figure 11. Comparison of the changes in the key structuring parameters as isocyanate conversion increases during the foaming reaction for RIMSAXS-210. SAXS relative invariant, Q' (△), hydrogen-bonded urea carbonyl, $[>C{=}O]_b/p_{NCO}$, (○), and elastic storage modulus, G' (+). The curve through the hydrogen-bonded urea carbonyl data is a fit to $[>C{=}O]_b/p_{NCO} = 1 - a[\exp(p_{NCO} - b)^c]$ according to a pseudo-Avrami analysis, where a, b, and c are fitting parameters. a is a rate constant, b is the conversion at the onset of hydrogen bonding, and c is the phase-growth exponent.

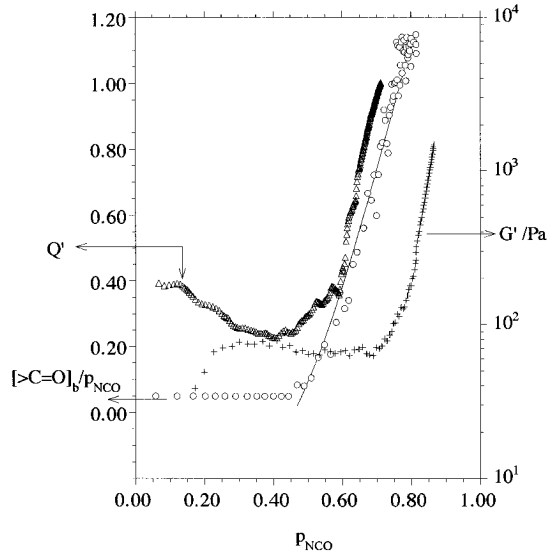

Figure 12. Comparison of the changes in the key structuring parameters as isocyanate conversion increases during the foaming reaction for RIMSAXS-210-MONOL. SAXS relative invariant, Q' (△), hydrogen-bonded urea carbonyl, $[>C{=}O]_b/p_{NCO}$, (○), and elastic storage modulus, G' (+). The curve through the hydrogen-bonded urea carbonyl data is a fit to $[>C{=}O]_b/p_{NCO} = 1 - a[\exp(p_{NCO} - b)^c]$ according to a pseudo-Avrami analysis, where a, b, and c are fitting parameters. a is a rate constant, b is the conversion at the onset of hydrogen bonding, and c is the phase-growth exponent.

concentration of hydrogen-bonded urea carbonyl species, $[>C{=}O]_b/p_{NCO}$ for the polyol system and *does* start to increase prior to the rapid growth in the concentration of hydrogen-bonded urea carbonyl species for the monol system. In both systems, the growth of the foam's elastic shear modulus, G', lags the growth of the relative invariant and the hydrogen-bonded urea carbonyls. A simplified analogy to this discussion is that microphase separation is considered to be the "closing of the door" on the system and the subsequent formation of the hydrogen bonds between the microphase-separated urea hard segments is the "turning of the door handle". i.e., the hydrogen bonds fix the structure in place. This is then further locked in place by vitrification of the hard segments as the Berghmans point is crossed,[37] i.e., the "turning of the key".

In order that an objective description of both the chemical and physical events taking place and, ultimately, selective control of the reactive processing of flexible polyurethane foam be achieved; *in-situ* investigations into both the reaction kinetics and the development of morphology *under processing conditions* are essential. The use of model systems has demonstrated that the presence of covalent cross-links delay the onset of microphase separation of the urea hard segment sequence lengths; however, in terms of dimensional stability and the mechanical/physical properties of the foam, molecular connectivity between the microphases via urethane covalent cross-links is essential.

Acknowledgment. M.J.E. and A.J.R. would like to thank Dow Benelux N.V., Terneuzen, The Netherlands, for suggesting this problem and providing the necessary financial support. The SERC provided beam time at the Daresbury SRS under Minor Grant 21/109. Finally, it is a pleasure to acknowledge the technical support of Wim Bras (NWO/AMOLF, The Netherlands), Steve Mortimer, and Ernie Komanscheck (Polymer Group, UMIST).

References and Notes

(1) Artavia, L. D.; Macosko, C. W. *J. Cell. Plast.* **1990**, *26*, 490.
(2) Priester, R. D., Jr.; McClusky, J. V.; O'Neill, R. E.; Turner, R. B.; Harthcock, M. A.; Davis, B. L. *J. Cell. Plast.* **1990**, *26*, 346.
(3) Artavia, L. D. Ph.D. Thesis, University of Minnesota, 1991.
(4) Elwell, M. J. A.; Ryan, A. J.; Grünbauer, H. J. M.; Van Lieshout, H. C.; Thoen, J. A. *Prog. Rubber. Plast. Technol.* **1993**, *9*, 120.
(5) Elwell, M. J. A. Ph.D. Thesis, Victoria University of Manchester, 1993.
(6) Turner, R. B.; Spell, H. L.; Wilkes, G. L. *Proc. 28th SPI Annu. Tech./Mrkt. Conf., 28th* **1988**, 244.
(7) Armistead, J. P.; Turner, R. B.; Wilkes, G. L. *J. Appl. Polym. Sci.* **1988**, *35*, 601.
(8) Creswick, M. W.; Lee, K. D.; Turner, R. B.; Huber, L. M. *J. Elast. Plast.* **1989**, *21*, 179.
(9) Ryan, A. J. *Polymer* **1990**, *31*, 707.
(10) Ryan, A. J.; Stanford, J. L.; Still, R. H. *Plast. Rubber Proc. Appl.* **1990**, *13*, 99.
(11) Grünbauer, H. J. M.; Thoen, J. A.; Folmer, J. C. W.; Van Lieshout, H. C. *J. Cell. Plast.* **1992**, *28*, 36.
(12) Elwell, M. J. A.; Ryan, A. J.; Mortimer, S. *Macromolecules* **1994**, *27*, 5428.
(13) Wong, S. W.; Frisch, K. C. *Prog. Rubber Plast. Technol.* **1991**, *7*, 243.
(14) Wong, S. W.; Frisch, K. C. *J. Polym. Sci., Part A: Polym. Chem.* **1986**, *24*, 2867.
(15) Sorokin, M. F.; Shode, L. G.; Klochkova, L. V.; Finyakin, L. N. *Izv. Vyssh. Uchebn. Zaved., Khim. Khim. Tekhnol.* **1984**, *27*, 852.
(16) Gus'kova, N. A.; Sorokin, M. F. *Deposited Doc.* **1978**, VINITI *12*, 321.
(17) Lipatova, T. E.; Bakalo, L. A.; Chirkova, L. I. *Sint. Fiz.-Khim. Polim.* **1978**, *23*, 74.
(18) Metlyakova, I. R.; Shoshtaeva, M. V. *Sint. Fiz.-Khim. Polim.* **1976**, *18*, 48.
(19) Borkent, G. *Adv. Urethane Sci. Technol.* **1974**, *3*, 1.
(20) Grigor'eva, V. A.; Baturin, S. M.; Entelis, S. G. *Vysokomol. Soedin., Ser. A.* **1972**, *14*, 1345.
(21) Rossmy, G. R.; Kollmeier, H. J.; Lidy, W.; Schator, H.; Wiemann, M. *J. Cell. Plast.* **1981**, *17*, 319.
(22) Rossmy, G. R.; Kollmeier, H. J.; Lidy, W.; Schator, H.; Wiemann, M. *J. Cell. Plast.* **1977**, *13*, 26.
(23) Rossmy, G. R.; Kollmeier, H. J.; Lidy, W.; Schator, H.; Wiemann, M. *J. Cell. Plast.* **1979**, *15*, 276.
(24) Hocker, J. *J. Appl. Polym. Sci.* **1980**, *25*, 2879.

(25) Elwell, M. J. A. *Thermochim. Acta* **1995**, *269*, 145.
(26) Macosko, C. W. *RIM: Fundamentals of Reaction Injection Molding*; Carl Hanser Verlag: Munich, 1988.
(27) Ryan, A. J.; Willkomm, W. R.; Bergstrom, T. B.; Macosko, C. W.; Koberstein, J. T.; Yu, C. C.; Russell, T. P. *Macromolecules*, **1991**, *24*, 2883.
(28) Mikkleson, K.; Macosko, C. W. *J. Cell. Plast.* **1989**, *21*, 29.
(29) Yang, W. P.; Macosko, C. W. *Makromol. Chem., Macromol. Symp.*, **1989**, *25*, 23.
(30) Mora, E.; Artavia, L. D.; Macosko, C. W. *J. Rheol.* **1991**, *35*, 921.
(31) Mora, E. M.Sc. Dissertation, University of Minnesota, 1991.
(32) Neff, R.; Macosko, C. W., unpublished results.
(33) Bailey, F. E.; Critchfield, F. E. *J. Cell. Plast.* **1981**, *17*, 333.
(34) Merten, R.; Lauerer, D.; Dahm, M. *J. Cell. Plast.* **1968**, *4*, 262.
(35) Elwell, M. J. A.; Ryan, A. J.; Grünbauer, H. J. M.; Van Lieshout, H. C., *Polymer*, in press.
(36) Elwell, M. J. A.; Ryan, A. J.; Grünbauer, H. J. M.; Van Lieshout, H. C.; Lidy, W. *Plast. Rubber Proc. Appl.* **1995**, *23*, 265.
(37) Callister, S.; Keller, A.; Hikmet, R. M. *Makromol. Chem., Macromol. Symp.* **1990**, *39*, 19.
(38) Connell, J. G.; Richards, R. W.; Rennie, A. R. *Polymer* **1991**, *32*, 2033.
(39) Olabisi, O.; Robeson, L. M.; Shaw, M. T. *Polymer-Polymer Miscibility;* Academic Press: New York, 1977.
(40) Binder, K. In *Phase Transformations in Materials*; Cahn, R. W., Haasen, P., Kramer, E. J., Eds.; Materials Science and Technology: A Comprehensive Treatment, VCH Publishers: Weinheim, 1991; Chapter 7, p 405.
(41) Hashimoto, T. *Macromolecules* **1987**, *20*, 465.
(42) Cahn, J. W.; Hilliard, J. *J. Chem. Phys.* **1958**, *28*, 258.
(43) Bates, F. S.; Wiltzius, P. *J. Chem. Phys.* **1989**, *91*, 3258.
(44) Kanner, B.; Decker, T. G. *J. Cell. Plast.* **1969**, *5*, 32.
(45) Khan, S. A.; Schnepper, C. A.; Armstrong, R. C. *J. Rheol.* **1988**, *32*, 69.
(46) Princen, H. M.; Kiss, A. D. *J. Colloid Interface Sci.* **1986**, *112*, 427.
(47) Bates, F. S. *Macromolecules* **1984**, *17*, 2607.
(48) Bates, F. S.; Rosedale, J. H.; Frederickson, G. H. *J. Chem. Phys.* **1990**, *92*, 6255.
(49) Rosedale, J. H.; Bates, F. S. *Macromolecules* **1990**, *23*, 2329.
(50) Ryan, A. J.; Macosko, C. W.; Bras, W. *Macromolecules* **1992**, *25*, 6277.
(51) Leibler, L. *Macromolecules* **1980**, *13*, 1602.
(52) Benoit, H.; Hadziioannou, G. *Macromolecules* **1988**, *21*, 1449.

MA9511208